Supporting Information

A highly stretchable, self-adhesive, antimicrobial conductive hydrogel with guar gum/acrylic acid/MXene@AgNPs for multifunctional wearable sensors and electromagnetic interference shielding

*Tongle Pu [a], Changgeng Li [b], Lin Yang [a], Xiu-zhi Tang [c], Yunjun Ruan [a], Tong Guo [a]**
a College of Big Data and Information Engineering, Guizhou University, Guiyang 550025, China
b School of Electronic Information, Central South University, Changsha 410083, China
c School of Aeronautics and Astronautics, Central South University, Changsha 410083, China
**Corresponding author. E-mail: tguo3@gzu.edu.cn (Tong Guo)*

1 Structure and Morphology of MXene@AgNPs

Employing silver nitrate as the silver source and MXene as the reducing agent, MXene@AgNPs were synthesized in situ through the self-chemical reduction method. The XRD patterns of MXene and MXene@AgNPs are depicted in Fig. S1. Specifically, MXene@AgNPs exhibit four distinct diffraction peaks at 38.3°, 44.5°, 64.4°, and 77.4°. These peaks correspond respectively to the (111), (200), (220), and (311) crystal planes of the face-centered cubic structure of silver, showing complete consistency with the silver standard card (PDF#65–2871). This finding indicates that the silver deposited on the surface of MXene exists in a pure elemental form. The SEM image of MXene@AgNPs, as illustrated in Fig. S2a-b, reveals a substantial number of AgNPs adhering to the MXene nanosheets and the inter-layer regions, with an average particle size of approximately 200 nm. Additionally, the elemental distribution map (Fig. S2c) demonstrates that the distribution of the Ag element corresponds to the particles observed in the SEM, thus confirming the presence of AgNPs on the surface of MXene.

To further validate the formation of AgNPs, UV-vis spectra was utilized to characterize MXene@AgNPs. As shown in Fig. S3, a strong absorption peak emerges at 217 nm, predominantly attributed to the electron transitions of MXene nanosheets

and the vibrations of surface functional groups. A relatively broad absorption peak is observed at 424 nm, and these absorption peaks are ascribed to the AgNPs generated by surface plasmon resonance (SPR), indicating the successful formation of AgNPs. In addition, AgNPs are embedded in the hydrogel network over extended periods, and their long-term stability is of great significance for the application of hydrogels in the biomedical field. Therefore, the stability of AgNPs inside the hydrogel was evaluated by UV-vis. As shown in Fig. S6, the UV-vis of the $GAMA_2$ hydrogel exhibited a relatively broad absorption peak at 417 nm on the first day of preparation. Remarkably, after 30 days of storage at room temperature, no discernible shift of this absorption peak at 417 nm was detected in the UV-vis of the $GAMA_2$ hydrogel. This observation strongly suggests that the AgNPs embedded in the hydrogel network possess excellent stability.

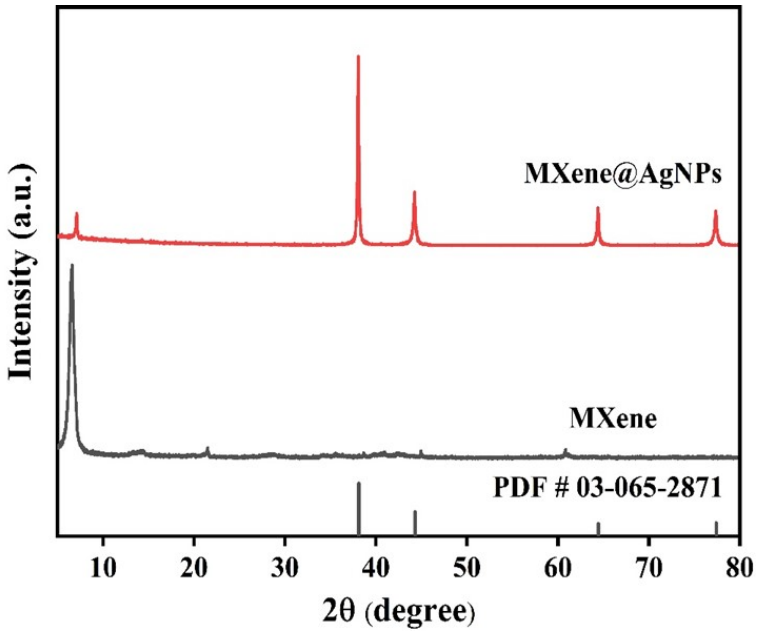

Fig. S1 XRD curves of the MXene and MXene@AgNPs.

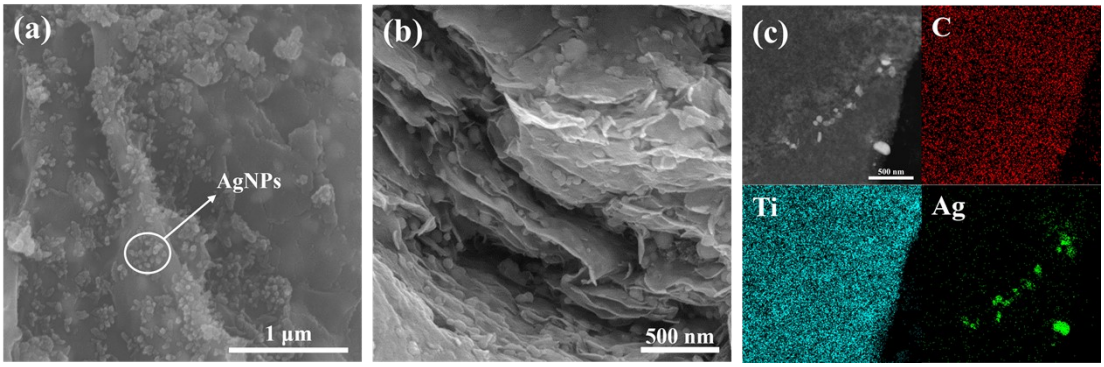

Fig. S2 Morphological Characterization of MXene@AgNPs. (a-b) SEM image of MXene@AgNPs and (c) corresponding EDS elemental mapping of MXene@AgNP

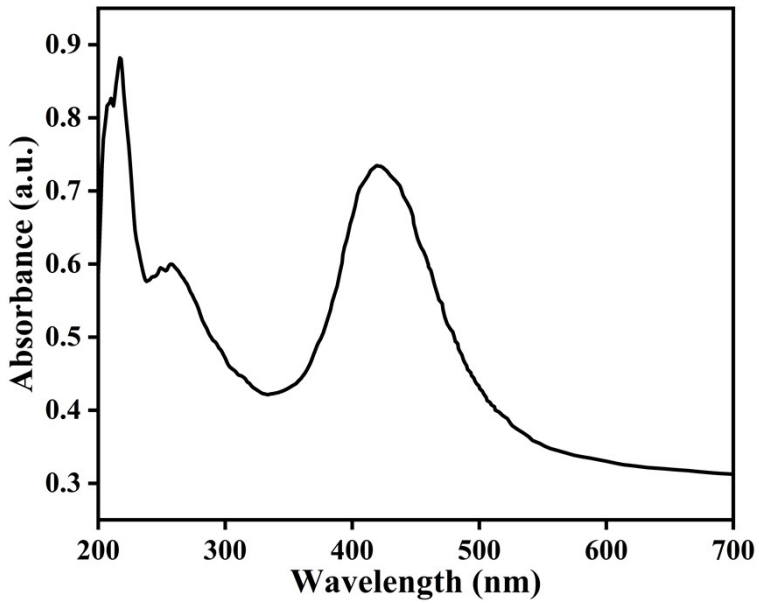

Fig. S3 UV–vis spectra of MXene@AgNPs.

2. Silver release behavior of GAMA$_2$ hydrogels

The release of silver from the hydrogel nanocomposites was tested in PBS at 37 °C. Each sample (10 mm × 10 mm × 0.2 mm) was immersed in 50 mL of PBS. The PBS was periodically replaced within 0-24 h to create an infinite sink solution. The released silver ions were quantified by atomic absorption spectrometry (Perkin Elmer, Analyst 100).

The silver release behavior in hydrogels, especially the concentration of the released silver, dictates the antibacterial behavior and cytotoxicity of antibacterial hydrogels. The silver release curves of the hydrogels are presented in Fig. S4. The GAM hydrogel,

without the addition of AgNPs, has a curve that nearly coincides with the horizontal axis, clearly indicating negligible silver ion release during the test period. In contrast, for the $GAMA_1$ and $GAMA_2$ hydrogels, due to the incorporation of AgNPs, the curves of both display an upward trend, which reflects the continuous release of silver ions. Notably, the $GAMA_2$ hydrogel contains a higher content of AgNPs than the $GAMA_1$ hydrogel. Throughout the entire test time span, the curve of the $GAMA_2$ hydrogel has a steeper slope, signifying a faster silver ion release rate, and its cumulative release amount is consistently higher. From the 4th to 7th day, the cumulative release amount of the $GAMA_2$ hydrogel stabilizes at approximately 7.45 ± 0.29 μg/mL, while that of the $GAMA_1$ hydrogel reaches a stable value of around 5.56 ± 0.33 μg/mL. This result reveals the significant impact of the addition or non-addition of AgNPs and the differences in the addition amount on the silver ion release behavior of hydrogels. It thus provides a crucial basis for evaluating the performance of these hydrogels in applications such as antibacterial and biomedical fields that necessitate silver ion release.

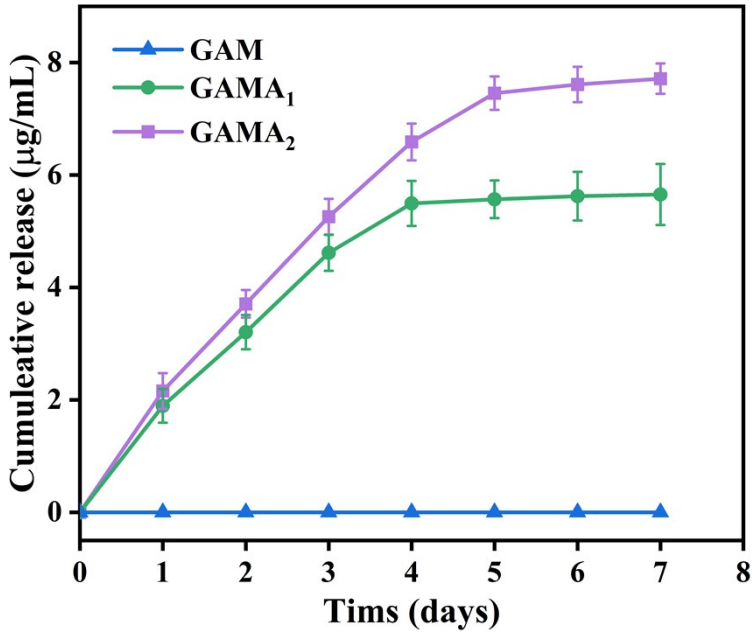

Fig. S4 The releasing profile of AgNPs vs time.

3. Degradation behavior of $GAMA_2$ hydrogel

In-vitro biodegradation behavior of the prepared hydrogel was evaluated by measuring the weight loss as a function of time. First, the initial weight of the $GAMA_2$ hydrogel

dried to a constant weight was accurately weighed. Then, it was immersed in phosphate-buffered saline (PBS) solution at 37 °C (pH: 7.4), and the PBS solution was replaced daily. At predetermined time intervals, the hydrogel samples were taken out from the PBS solution, washed with distilled water, and then dried in an oven at 60 °C until a constant weight was obtained. The weight of the hydrogel at this time was recorded. The degradation rate of the hydrogel was calculated using Equation (1):

$$Weight\ loss\ (\%) = \frac{W_0 - W_t}{W_0} \times 100\%\#(1)$$

In order to evaluate the degradation characteristics of the $GAMA_2$ hydrogel, the hydrogel was immersed in PBS solution to measure the weight loss. As shown in Fig. S5, within 21 days, the mass loss of the hydrogel in the PBS solution was more than 80%, indicating that the $GAMA_2$ hydrogel could undergo significant degradation within 21 days. This degradation is primarily attributed to the functional groups on the surface of MXene nanosheets and the carboxyl groups of PAA, which impart high hydrophilicity to the $GAMA_2$ hydrogel. This hydrophilicity results in excessive water absorption, ultimately leading to structural collapse after swelling.

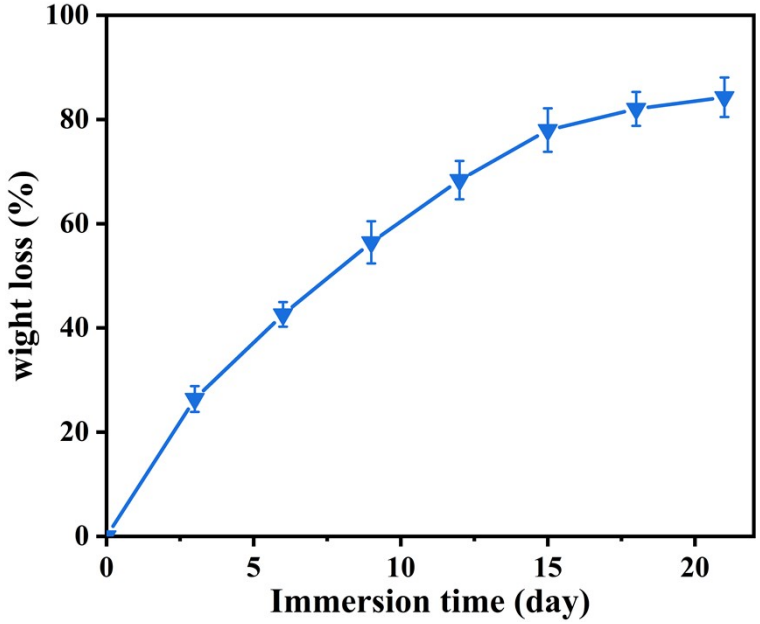

Fig. S5 Degradation rate of the $GAMA_2$ hydrogel in PBS.

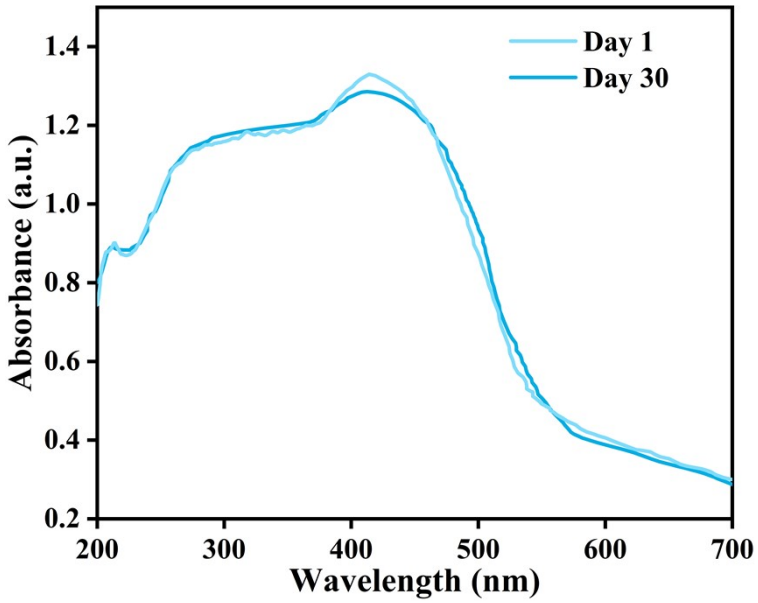

Fig. S6 UV-vis spectra of the $GAMA_2$ hydrogel after 30 days of preparation.

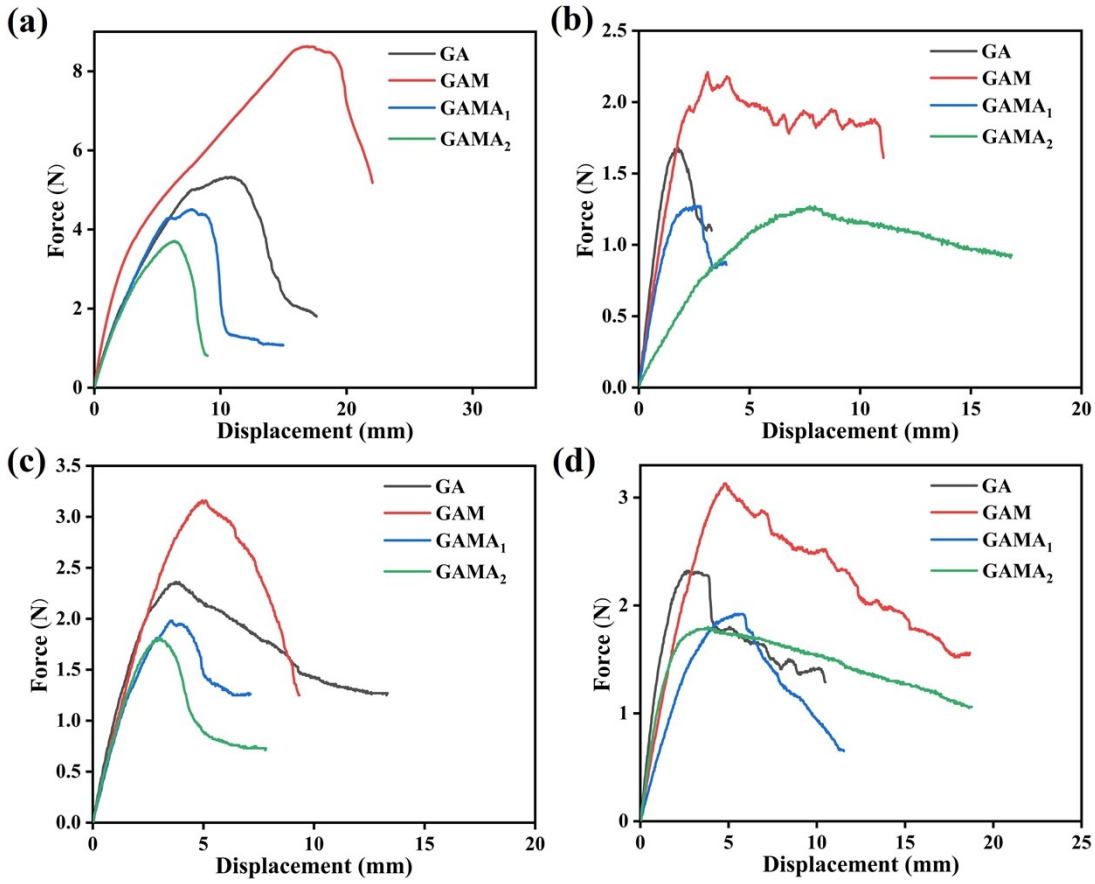

Fig. S7 Adhesion-displacement curves of different hydrogels to wood, glass, copper and PTFE.

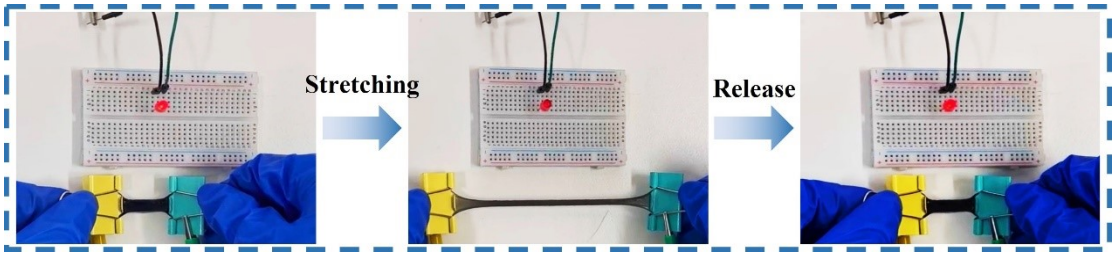

Fig. S8 Optical picture of stretching conductivity of $GAMA_2$ hydrogel.

Table S1. The comparison of GAMA hydrogel and recently reported hydrogels.

Samples	Stretchability (%)	EMI SE (dB)	Conductivity (mS cm^{-1})	GF	Biosafety	Ref
PVA/glycerol/NaCl	500	N/A	7.2	1.23	N/A	1
PNIPAAm/PANI	290	N/A	0.68	3.92	N/A	2
TA@Fe^{3+}–PAA	3560	24.5	335.8	2.11	Antibacterial	3
TAPU/Fe_3O_4@TA	371	26	0.36	2.07	N/A	4
LMCNF	520.45	33.1	256.9	2.92	Antibacterial	5
TA-Fe_3O_4@MXene-PSBMA/AM	308.5	25.2	13.3	2.38	N/A	6
PVA/PA/MXene	271.43	N/A	N/A	3.23	N/A	7
PVA/TA@s-NC	1211	N/A	3.16	4.75	Antibacterial Biocompatibility	8
PVA-CT-Ag-Al-Gly	350.54	N/A	N/A	1.6	Antibacterial Biocompatibility	9
GAMA	**850**	**34.5**	**14.04**	**6.48**	**Antibacterial Biocompatibility**	**This work**

References

1 S. Li, H. Pan, Y. Wang and J. Sun, *J. Mater. Chem. A*, 2020, **8**, 3667–3675.

2 Z. Wang, H. Zhou, W. Chen, Q. Li, B. Yan, X. Jin, A. Ma, H. Liu and W. Zhao, *ACS Appl. Mater. Interfaces*, 2018, **10**, 14045–14054.

3 G. Miao, L. Xu, F. Li, X. Miao, Z. Hou, T. Xu, G. Ren, X. Yang, J. Qiu and X. Zhu, *Langmuir*, 2023, **39**, 10530–10541.

4 Y. Liu, Z. Zhang, X. Yang, F. Li, Z. Liang, Y. Yong, S. Dai and Z. Li, *J. Mater. Chem. A*, 2023, **11**, 6603–6614.

5 X. Feng, C. Wang, S. Shang, H. Liu, X. Huang, J. Jiang, Z. Song and H. Zhang, *Carbohydr. Polym.*, 2023, **311**, 120786.

6 H. Sima, B. Liu, X. Shi, Z. Zhao, C. Liu and C. Zhang, *Colloids Surf. Physicochem. Eng. Asp.*, 2024, **702**, 135028.

7 X. Zhao, H. Jiang, P. Sun, R. Wei, S. Jiang, J. Hu and S. Zhang, *ACS Appl. Mater. Interfaces*, 2023, **15**, 56275–56284.

8 D. K. Patel, K. Ganguly, S. D. Dutta, T. V. Patil, A. Randhawa and K.-T. Lim, *Int. J. Biol. Macromol.*, 2023, **229**, 105–122.

9 B. Song, X. Fan and H. Gu, *ACS Appl. Mater. Interfaces*, 2023, **15**, 2147–2162.